PHYSICAL REVIEW MATERIALS **7**, 124601 (2023)

Effect of Mn substitution on the electronic structure for Mn-doped indium-tin oxide films studied by soft and hard x-ray photoemission spectroscopy

Daiki Ootsuki,[1,*] Tatsuhiro Ishida,[1] Naoya Tsutsumi,[1] Masaki Kobayashi,[2,3] Kohdai Inagaki,[2] Teppei Yoshida,[1]
Yukiharu Takeda,[4] Shin-ichi Fujimori,[4] Akira Yasui,[5] Saiki Kitagawa,[1] and Toshihiro Nakamura[1,6]
[1]*Graduate School of Human and Environmental Studies, Kyoto University, Sakyo-ku, Kyoto 606-8501, Japan*
[2]*Department of Electrical Engineering and Information Systems, The University of Tokyo, 7-3-1 Hongo, Bunkyo-ku, Tokyo 113-8656, Japan*
[3]*Center for Spintronics Research Network, The University of Tokyo, 7-3-1 Hongo, Bunkyo-ku, Tokyo 113-8656, Japan*
[4]*Materials Sciences Research Center, Japan Atomic Energy Agency, Sayo-gun, Hyogo 679-5148, Japan*
[5]*SPring-8/JASRI, 1-1-1 Koto, Sayo-cho, Hyogo 679-5198, Japan*
[6]*Institute for Liberal Arts and Sciences, Kyoto University, Yoshida Nihonmatsu-cho, Sakyo-ku, Kyoto 606-8501, Japan*

(Received 7 August 2023; accepted 28 November 2023; published 18 December 2023)

We report the electronic structure of $In_{1.8-x}Mn_xSn_{0.2}O_3$ ($x = 0.0$, 0.2, and 0.3), which combines transparency, ferromagnetism, and semiconducting properties, by means of hard x-ray photoemission spectroscopy (HAXPES), soft x-ray resonant photoemission spectroscopy (RPES), and x-ray absorption spectroscopy (XAS). The spectral shape of the Mn *L*-edge XAS spectra indicates that the valence of the substitutional Mn ions is divalent. The peak position of the In 3*d* and O 1*s* core-level spectra shifts toward lower binding energy with Mn concentration suggest the hole doping due to the Mn^{2+} ions. The valence-band spectra exhibit the well-defined features associated with the donor states across the Fermi level E_F and the valence-band edge. The valence-band maximum (VBM) shifts to lower binding energy and the spectral weight near E_F decreases with increasing Mn concentration, which is consistent with the hole doping nature observed in the core-level shift. The Mn 2*p*-3*d* RPES reveals that the hump structure around 1.9 eV above the VBM originates from the Mn 3*d* impurity band and the valence-band state consists of the O 2*p* band strongly hybridized with the Mn 3*d* orbital. Furthermore, there is no contribution of the Mn 3*d* orbital to the spectral weight close to E_F. Our results reveal the entire valence-band structure of $In_{1.8-x}Mn_xSn_{0.2}O_3$ and the effect of the Mn substitution, which provides the important information related to the physical properties such as transparency, electrical conductivity, and ferromagnetism for the functional materials.

DOI: 10.1103/PhysRevMaterials.7.124601

I. INTRODUCTION

Impurity states by substitution of the cation site play an important role for the fascinating properties of the semiconducting materials such as high conductivity, transparency, and ferromagnetism. It is crucial to describe how the electronic state is changed by impurity substitution and is expected to provide a guideline for material design. The doped ions form a textbook hydrogenic impurity state and its energy level is located in the vicinity of the conduction-band bottom or the valence-band top, which is so-called shallow impurity state [1]. On the other hand, the deep impurity state due to the doped transition metal has been discussed intensively. Haldane and Anderson have shown that the multiple charge state is formed within the band gap of semiconductors [2], and the systematic variation of the charge state with chemical trend has been studied [3–6]. Furthermore, the vacuum pinning rule of the transition-metal impurity state and the bound state induced by the negative Coulomb interaction have also been discussed [7–11]. Thus, the electronic state of the isolated transition-metal impurity in semiconductors has been the subject of much debate.

Indium-tin oxide $In_{2-x}Sn_xO_3$ is one of the most important materials in the transparent semiconductors using the applications such as transparent electrodes of flat panel displays, organic light emitting diodes, and solar cells [12–14]. The crystal structure of the pristine In_2O_3 is the cubic-bixbyite type structure as shown in Fig. 1(a). In_2O_3 has filled O 2*p* orbitals of O^{2-} ions and empty In 5*s* orbitals of In^{3+} ions [15], showing the direct band gap ≈2.9 eV [16–20]. The carrier concentration and the electrical resistivity can be controlled by Sn substitution for In site as well as the oxygen vacancy [13,15,21]. Here, the In^{3+} ion is replaced to the Sn^{4+} ion. The substitutional Sn impurity forms the donor level and injects the Sn 5*s* electrons into In_2O_3. Previous Mössbaur spectroscopy and x-ray and neutron diffraction studies proposed that the oxygen coordination surrounding the substitutional Sn ion strongly depends on the doping concentration [22–24]. For the low-doping region, the Sn^{4+} ion is coordinated by six oxygen anions, which is so-called *b* site and *d* site according to the Wyckoff's notation [Fig. 1(b)]. On further doping, the seven- or eight-coordinated Sn^{4+} ion is realized. The only six-coordinated Sn^{4+} can introduce the electrons into the system. Moreover, the high-temperature ferromagnetism in $In_{2-x}Sn_xO_3$ has been reported by adding the spin degree of freedom due to the transition-metal impurity [25–36]. Nakamura *et al.* have successfully synthesized $In_{2-x-y}Mn_xSn_yO_3$

---

[*] ootsuki.daiki.4z@kyoto-u.ac.jp

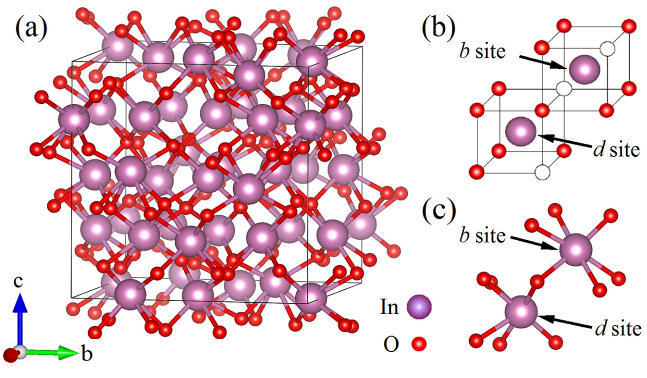

FIG. 1. (a) Crystal structure of the cubic-bixbyite type structure In_2O_3 and (b), (c) schematics of the *b* site and *d* site in the bixbyite structure visualized by VESTA [38]. The open circle indicates the structural vacancy.

films on substrates showing ferromagnetism, low electrical resistivity of the order of 10^{-4} Ω cm, and high optical transmittance by using the radio frequency (rf) magnetron sputtering methods [28,29,37]. The variation of the electronic structure by the impurity doping, however, remains to be clarified in spite of possessing all the important properties for the device application.

In this study, we have investigated the electronic structure of $In_{1.8-x}Mn_xSn_{0.2}O_3$ by means of the hard x-ray photoemission spectroscopy (HAXPES), the soft x-ray resonant photoemission spectroscopy (RPES), and the x-ray absorption spectroscopy (XAS) in order to reveal the effect of Mn substitution for the electronic state. The divalent state of the substitutional Mn ions has been determined by the Mn *L*-edge XAS spectra. The In 3*d* and O 1*s* core-level spectra are slightly shifted toward lower binding energy with Mn^{2+} substitution in contrast with the Sn 3*d* core level. Moreover, the finite intensity around the Fermi level E_F and the spectral onset around the binding energy E_B of 2.8 eV in the valence-band spectra are corresponding to the donor state formed by Sn substitution and the valence-band edge, respectively. The valence-band maximum (VBM) shifts to lower binding energy and the spectral intensity at E_F decreases with Mn doping, suggesting the hole doping due to the Mn^{2+} substitution. In addition, the hump structure around $E_B = 1.9$ eV was observed above the VBM. To extract the partial density of states of the Mn 3*d* orbital in the valence band, we have performed the Mn 2*p*-3*d* RPES for $In_{1.8-x}Mn_xSn_{0.2}O_3$. The RPES revealed that the hump structure is originating from the Mn 3*d* states and the observed spectral weight at E_F is negligibly hybridized with the Mn 3*d* states. In addition, the valence-band structure is strongly hybridized with the O 2*p* band and the Mn 3*d* orbitals.

II. EXPERIMENTAL SETUPS

Mn-doped indium-tin oxide films $In_{1.8-x}Mn_xSn_{0.2}O_3$ ($x = 0.0$, 0.2, and 0.3) were grown epitaxially by the rf magnetron sputtering on yttria-stabilized zirconia (111) substrates [39,40]. The carrier concentrations were estimated to be 2.83×10^{20} cm^{-3} for $x = 0.0$, 1.42×10^{20} cm^{-3} for $x = 0.2$, and 7.52×10^{18} cm^{-3} for $x = 0.3$ from Hall effect measurements [41].

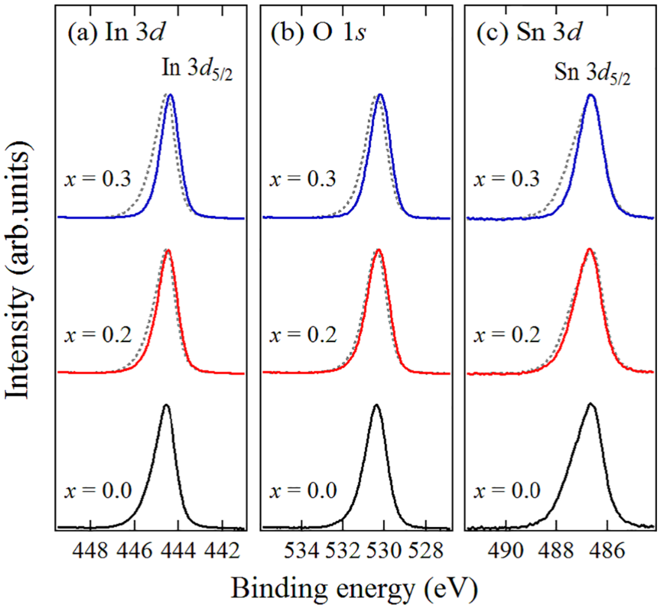

FIG. 2. Core-level photoemission spectra of (a) In 3*d*, (b) O 1*s*, and (c) Sn 3*d* for $In_{1.8-x}Mn_xSn_{0.2}O_3$ ($x = 0.0$, 0.2, and 0.3) films. The dashed curves indicate the replica of the spectra of $x = 0.0$. The data were collected at $h\nu = 7940$ eV.

Soft x-ray RPES and XAS measurements were performed at BL23SU at SPring-8 with a Scienta SES2002 electron analyzer. The incident photon energy was set to $h\nu = 635$–660 eV. The total-energy resolution was about 180 meV for circularly polarized light $h\nu = 635$–660 eV. The measurement chamber was maintained in ultrahigh vacuum of higher than 1.5×10^{-10} Torr. HAXPES measurements were carried out at BL09XU of SPring-8 with a Scienta R4000 electron analyzer [42]. The incident photon energy was set to $h\nu = 7940$ eV with the linear polarized light. The total-energy resolution was 190 meV for $h\nu = 7940$ eV. The base pressure of the chamber was 1.0×10^{-10} Torr. The data were collected at $T = 300$ K without surface treatment because of the large probing depth of hard x-rays. For the relatively surface-sensitive soft x-ray region, we have confirmed that the there is no additional structure due to the surface contamination. The binding energy was calibrated by using the Fermi edge of the gold reference.

III. RESULTS AND DISCUSSION

Figures 2(a)–2(c) show the core-level photoemission spectra taken at $h\nu = 7940$ eV. The In 3$d_{5/2}$ core level for $In_{1.8}Sn_{0.2}O_3$ ($x = 0.0$) is located at $E_B = 444.56$ eV and that of the O 1*s* core level is located at $E_B = 530.35$ eV, as shown in Figs. 2(a) and 2(b). The binding energies of those core levels agree with the previous results of In_2O_3, indicating that the valence state of In is trivalent In^{3+}: $4d^{10}5s^05p^0$ [15]. Considering more carefully, however, there are slight difference of the peak positions between $In_{1.8}Sn_{0.2}O_3$ and In_2O_3. The binding energies of In 3$d_{5/2}$ and O 1*s* for $In_{1.8}Sn_{0.2}O_3$ are higher than those of ≈444.4 eV and ≈530.2 eV for the previous HAXPES results of the pristine

In_2O_3, respectively [43–45]. These positive shifts suggest the variation of the chemical potential $\Delta\mu$, that is, the electron doping by Sn substitution. On the other hand, the Sn $3d_{5/2}$ core level of $In_{1.8}Sn_{0.2}O_3$ is located at $E_B = 486.65$ eV, as shown in Fig. 2(c), which is distinctly lower than that at $E_B \approx 487.1$ eV of $Sn^{4+}O_2$: $4d^{10}5s^05p^0$ and higher than that at $E_B \approx 486.2$ eV of $Sn^{2+}O$: $4d^{10}5s^25p^0$ [46,47]. The peak position of Sn $3d_{5/2}$ for $In_{1.8}Sn_{0.2}O_3$ is located at the middle of that between Sn^{4+} and Sn^{2+}. It is well known that the Sn ion is a valence skipper; that is, the tetravalent Sn^{4+} and the divalent Sn^{2+} are stable. As one possibility, the screening effect due to the Sn 5s electron localized around the substitutional Sn^{4+} ion can be considered. The doped electrons have the nature of Sn 5s orbital and the Sn 5s electron screens the Sn 3d core hole, since the substitutional Sn ions form the donor state below the In 5s conduction band across E_F. The resultant position of the Sn 3d core level of $In_{1.8}Sn_{0.2}O_3$ shifts from that of Sn^{4+} toward lower binding energy. Thus, the Sn ions are expected to inject the Sn 5s electrons into In_2O_3. Actually, the screening effect also can be seen in the lineshape of Sn 3d core level. The spectral shape of Sn 3d becomes asymmetric, since the asymmetric lineshape is due to the screening effect of the conductive electrons [48].

As for the Mn substitution, the In 3d and O 1s core-level spectra of $In_{1.8-x}Mn_xSn_{0.2}O_3$ in Figs. 2(a) and 2(b) are shifted toward the lower binding energy in going from $x = 0.0$ to 0.3, indicating the hole doping. In contrast, the peak positions of the Sn 3d core-level spectra do not change with the Mn doping as shown in Fig. 2(c). Figure 3 shows the Mn doping dependence of the XAS spectra for $In_{1.8-x}Mn_xSn_{0.2}O_3$ compared with the other Mn oxides. The observed Mn-L edge spectra for $In_{1.8-x}Mn_xSn_{0.2}O_3$ are very similar to that for MnO and are completely different from that for Mn metal, Mn_2O_3, and MnO_2. Judging from the comparison of the Mn L-edge spectra, it is concluded that the valence of Mn in $In_{1.8-x}Mn_xSn_{0.2}O_3$ is the divalent Mn^{2+}, dominantly. Thus, the substitutional Mn^{2+} ion acts as acceptor providing the hole into $In_{1.8-x}Mn_xSn_{0.2}O_3$. These results are entirely consistent with the shifts of the binding energies for the In 3d and O 1s core-levels with increasing Mn concentration.

The valence-band photoemission spectra measured at $h\nu = 7940$ eV are displayed in Fig. 4(a) and are basically consistent with the previous photoemission spectra of In_2O_3 [18,53,54]. The VBM is determined by the linear extrapolation of the valence-band edge. The energy of the VBM decreases from $E_B = 2.80$ to 2.61 eV with increasing x, which suggests the hole doping by Mn^{2+} substitution. Here, we compare the VBM with the core-level shifts with Mn doping as shown in Fig. 4(b). The variation of the VBM is quantitatively in good agreement with the shifts of the In 3d and O 1s core-levels, while the Sn 3d core-level exhibits a different behavior. Figure 4(c) shows the near-E_F spectra of $In_{1.8-x}Mn_xSn_{0.2}O_3$ ($x = 0.0$, 0.2, and 0.3), which is the enlarged view of Fig. 4(a). The spectral weight close to E_F is weakened in going from $x = 0.0$ to 0.3. Here, we discuss that there is no shift of the Sn 3d core levels with Mn doping. For $x = 0.0$, the donor state crosses E_F and the bound Sn 5s electrons around the substitutional Sn ions with a net positive charge strongly screen the Sn 3d core hole rather than the other core levels. The screening effect works toward shifting the Sn 3d core

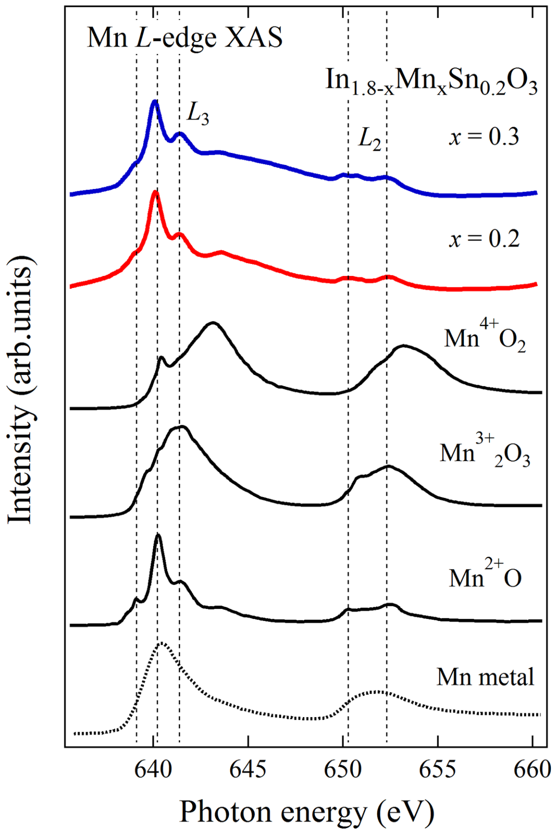

FIG. 3. Mn L-edge XAS spectra for $In_{1.8-x}Mn_xSn_{0.2}O_3$ ($x = 0.2$, and 0.3) films compared with that of Mn metal, MnO, Mn_2O_3, and MnO_2 [49–52]. The reference data were shifted to allow for a better comparison.

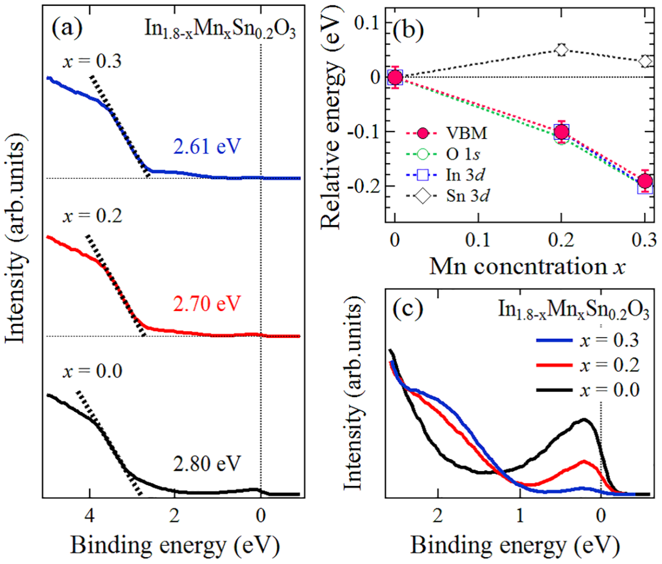

FIG. 4. (a) Leading edge of the valence-band photoemission spectra for $In_{1.8-x}Mn_xSn_{0.2}O_3$ ($x = 0.0$, 0.2, and 0.3) films. The data were taken at $h\nu = 7940$ eV. The linear extrapolations were used to deduce the VBM. (b) Relative energy shift of the In 3d, Sn 3d, and O 1s core levels compared with that of the energy of the VBM. (c) Enlarged view of the near-E_F spectra of panel (a).

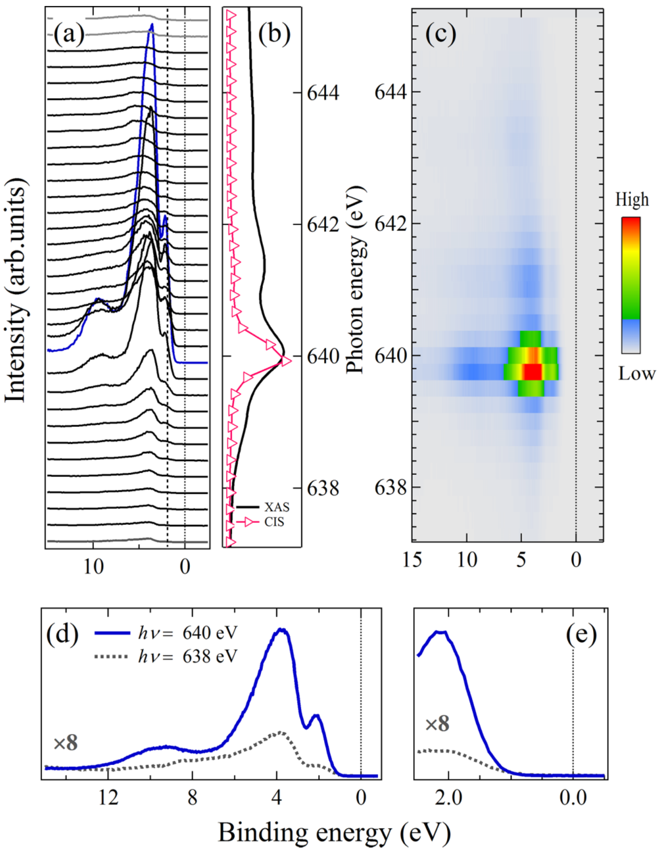

FIG. 5. (a) Mn $2p$-$3d$ RPES spectra of $In_{1.8-x}Mn_xSn_{0.2}O_3$ ($x = 0.3$) film. The data were collected from $h\nu = 637$ to 645 eV with the circularly polarized light. The each photoemission spectrum was angle-integrated. (b) X-ray absorption Mn L-edge spectra for $In_{1.8-x}Mn_xSn_{0.2}O_3$ ($x = 0.3$) film compared with CIS spectra taken from the intensity around 1.9 eV of panel (a). (c) Image plot of the resonant valence-band spectra of panel (a). (d) On- and off-resonance spectra at $h\nu = 640$ eV and 638 eV, respectively. (e) Enlarged view of the near-E_F spectra. The intensity of the off-resonance spectra is multiplied by eight for easy comparison.

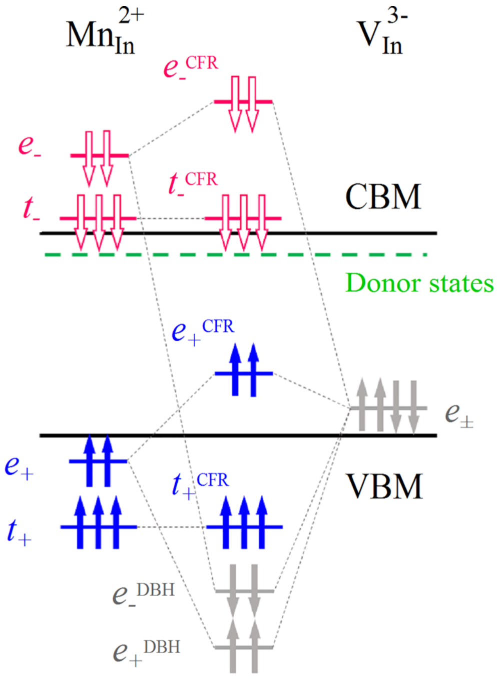

FIG. 6. Schematic diagram of the single-particle levels for the Mn $3d$ levels of the substitutional Mn^{2+} ions to the cation In^{3+} sites in $In_{1.8-x}Mn_xSn_{0.2}O_3$. The Mn $3d$ levels split into the spin configuration $t_\pm$ and $e_\pm$ levels and the $e_\pm$ levels are hybridized with host dangling-bond states (DBH). The In vacancy is denoted by V_{In}^{3-}. The dashed line indicates the donor state for the substitutional Sn ions and/or the oxygen vacancy. The figure has been made based on the theoretical calculation reported by Raebiger *et al.* [55].

level to the lower binding energy side. The Mn^{2+} substitution relaxes the screening effect through the reduction of the spectral weight at E_F due to the hole doping, and the Sn $3d$ core level should be shifted to the higher binding energy. However, the hole doping due to the substitutional Mn^{2+} induces the shift of the Sn $3d$ core level to the lower binding energy side. The core-hole screening effect and the hole-doping effect compensate each other thereby making the different shifts of the Sn $3d$ core level with Mn doping from those of In $3d$ and O $1s$. In addition, the suppression of the spectral weight at E_F causes the reduction of the asymmetric lineshape of the core level with Mn doping as shown in Fig. 2. Here, it should be noted that the bump around $E_B = 1.9$ eV for the photoemission spectra of Fig. 4(c) is enhanced in the Mn-doped samples of $x = 0.2$ and 0.3.

For the purpose of examining the nature of the structures around $E_B = 1.9$ eV as we mentioned in Fig. 4(c) and the effect of the Mn^{2+} substitution to the valence-band, we have performed the Mn $2p$-$3d$ RPES for $In_{1.8-x}Mn_xSn_{0.2}O_3$ ($x = 0.3$). Figure 5(a) shows the photon energy dependence of the valence-band spectra. The valence-band spectra strongly depend on the photon energy. To clarify the resonant structure, we plot a constant-initial-state (CIS) spectrum from the spectral intensity around $E_B = 1.9$ eV in Fig. 5(b). The CIS spectrum is clearly observed and agrees with the Mn L_3-edge x-ray absorption spectrum, indicating that the structure around $E_B = 1.9$ eV is originating from the Mn component. The image plot of Fig. 5(a) is displayed in Fig. 5(c) and exhibits the Mn $2p$-$3d$ resonant behavior in the wide region of the valence band. Here, the on- and off-resonant spectra for $h\nu = 640$ and 638 eV were determined from the CIS spectrum, respectively. The on-resonant spectral weight is widely distributed in the region from $E_B = 1$ to 14 eV. These results suggest that the substitutional Mn^{2+} is strongly hybridized with the O $2p$ orbital. On the contrary, there is no finite intensity close to E_F, that is, the absence of the Mn contribution near E_F as shown in Fig. 5(e).

Single-particle defect levels formed by substitution of the transition metal for the In^{3+} site in In_2O_3 were calculated by Raebiger *et al.* [55]. The Mn $3d$ orbital for the substitutional Mn ions splits into the crystal-field levels of e_g and t_{2g} orbitals, reflecting the nearly octahedral symmetry [Figs. 1(b) and 1(c)]. These levels further split into the spin configuration $t_\pm$ and $e_\pm$ levels and the doubly degenerate $e_\pm$ levels are hybridized with host dangling-bond states (DBH), as shown in Fig. 6. For the Mn^{2+} ion, the calculated crystal-field resonance (CFR) states (e_+^{CFR} levels) lie between the valence band and the conduction band, and the t_+^{CFR} states are fully occupied and located in the valence band, namely $t_+^3 e_+^2$. We speculate that the feature around 1.9 eV derived from the Mn 3*d* orbital corresponds to the e_+^2 states.

Our spectroscopic findings reveal that the substitutional Mn^{2+} ions act as the hole dopant and inject the hole into the system. This suggests that the Mn substitution can control the number of carriers with keeping the transparency. However, the reduction of the number of carriers due to the Mn substitution indicates the compensation of the electron doping from the donor state by Sn substitution and the hole doping by Mn substitution. Moreover, the Mn 3*d* orbital is strongly hybridized with the O 2*p* orbital mainly consisting of the valence band state, and there is no contribution of the substitutional Mn 3*d* orbital at E_F. These results would be informative for the functional material design and provide the important implications for the dilute ferromagnetism that has been reported in many indium-tin oxide system.

IV. CONCLUSION

We have performed HAXPES and XAS on $In_{1.8-x}Mn_xSn_{0.2}O_3$ films in order to investigate the electronic structure and the effect of the Mn substitution. From the Mn *L*-edge XAS spectra, we found the divalent state of the substitutional Mn ions. The Mn substitution induces the shifts toward the lower binding energy of VBM, suggesting the hole doping. Moreover, we have performed the Mn 2*p*-3*d* RPES to reveal the contribution of the valence band from the substitutional Mn ions. The resultant RPES spectra show that the valence-band structure at $E_B = 1.9$ eV within the band gap between the In 5s and/or Sn 5*s* conduction band and the O 2*p* valence band is originating from the Mn 3*d* orbital. Moreover, there is no contribution of the Mn 3*d* orbitals at E_F, while the Mn^{2+} ions are strongly hybridized with the O 2*p* orbital. Our spectroscopic results provide useful insights into $In_{1.8-x}Mn_xSn_{0.2}O_3$ showing transparency, high electrical conductivity, and ferromagnetism.

ACKNOWLEDGMENTS

The authors would like to thank M. Matsuki and M. Nagamoto for experimental support. This work was supported by the Japan Society for the Promotion of Science (JSPS) Grants-in-Aid for Scientific Research (KAKENHI No. JP20H01861, No. JP21K13882, No. JP22H02120, and No. JP23KJ1266). This work was partially supported the Spintronics Research Network of Japan (Spin-RNJ). The synchrotron radiation experiments were performed with the approval of SPring-8 (Proposal No. 2017A1406, No. 2019A3841, No. 2022A1579, No. 2022A1729, No. 2022A3841, No. 2022B1765, and No. 2023A1802). This work was partially performed under the Shared User Program of Japan Atomic Energy Agency (JAEA) Facilities (Proposal No. 2022A-E23) supported by JAEA Advanced Characterization Nanotechnology Platform as a program of "Nanotechnology Platform" of Ministry of Education, Culture, Sports, Science and Technology (MEXT) (Proposal No. JPMXP1222AE0022).

---

[1] W. Kohn, Solid State Phys. **5**, 257 (1957).
[2] F. Haldane and P. W. Anderson, Phys. Rev. B **13**, 2553 (1976).
[3] A. Zunger and U. Lindefelt, Solid State Commun. **45**, 343 (1983).
[4] H. Katayama-Yoshida and A. Zunger, Phys. Rev. B **31**, 8317 (1985).
[5] H. Raebiger, S. Lany, and A. Zunger, Nature (London) **453**, 763 (2008).
[6] T. Mizokawa and A. Fujimori, Phys. Rev. B **48**, 14150 (1993).
[7] L. A. Ledebo and B. K. Ridley, J. Phys. C: Solid State Phys. **15**, L961 (1982).
[8] M. J. Caldas, A. Fazzio, and A. Zunger, Appl. Phys. Lett. **45**, 671 (1984).
[9] A. Zunger, Phys. Rev. Lett. **54**, 849 (1985).
[10] P. W. Anderson, Phys. Rev. Lett. **34**, 953 (1975).
[11] H. Katayama-Yoshida and A. Zunger, Phys. Rev. Lett. **55**, 1618 (1985).
[12] C. G. Granqvist and A. Hultaker, Thin Solid Films **411**, 1 (2002).
[13] I. Hamberg and C. G. Granqvist, J. Appl. Phys. **60**, R123 (1986).
[14] G. Gu, V. Bulovic, P. E. Burrows, S. R. Forrest, and M. E. Thompson, Appl. Phys. Lett. **68**, 2606 (1996).
[15] John C. C. Fan and John B. Goodenough, J. Appl. Phys. **48**, 3524 (1977).
[16] R. L. Weiher and R. P. Ley, J. Appl. Phys. **37**, 299 (1966).
[17] A. Bourlange, D. J. Payne, R. G. Egdell, J. S. Foord, P. P. Edwards, M. O. Jones, A. Schertel, P. J. Dobson, and J. L. Hutchison, Appl. Phys. Lett. **92**, 092117 (2008).
[18] A. Walsh, J. L. F. Da Silva, S.-H. Wei, C. Körber, A. Klein, L. F. J. Piper, Alex DeMasi, Kevin E. Smith, G. Panaccione, P. Torelli, D. J. Payne, A. Bourlange, and R. G. Egdell, Phys. Rev. Lett. **100**, 167402 (2008).
[19] F. Fuchs and F. Bechstedt, Phys. Rev. B **77**, 155107 (2008).
[20] P. D. C. King, T. D. Veal, F. Fuchs, Ch. Y. Wang, D. J. Payne, A. Bourlange, H. Zhang, G. R. Bell, V. Cimalla, O. Ambacher, R. G. Egdell, F. Bechstedt, and C. F. McConville, Phys. Rev. B **79**, 205211 (2009).
[21] G. Frank and H. Köstlin, Appl. Phys. A: Solids Surf. **27**, 197 (1982).
[22] N. Yamada, I. Yasui, Y. Li, and YusukeUjihira Nomura, Jpn. J. Appl. Phys. **38**, 2856 (1999).
[23] N. Yamada, I. Yasui, Y. Shigesato, H. Li, Y. Ujihira, and K. Nomura, Jpn. J. Appl. Phys. **39**, 4158 (2000).
[24] G. B. González, J. B. Cohen, J.-H. Hwang, and T. O. Mason, J. Appl. Phys. **89**, 2550 (2001).
[25] H. S. Kim, S. H. Ji, H. Kim, S.-K. Hong, D. Kim, Y. E. Ihm, and W. K. Choo, Solid State Commun. **137**, 41 (2006).
[26] J. Philip, A. Punnoose, B. I. Kim, K. M. Reddy, S. Layne, J. O. Holmes, B. Satpati, P. R. LeClair, T. S. Santos, and J. S. Moodera, Nat. Mater. **5**, 298 (2006).
[27] J. Philip, N. Theodoropoulou, G. Berera, and J. S. Moodera, Appl. Phys. Lett. **85**, 777 (2004).
[28] T. Nakamura, K. Tanabe, K. Tsureishi, and K. Tachibana, J. Appl. Phys. **101**, 09H105 (2007).
[29] T. Nakamura, S. Isozaki, K. Tanabe, and K. Tachibana, J. Appl. Phys. **105**, 07C511 (2009).

[30] Y. K. Yoo, Q. Z. Xue, H. C. Lee, S. F. Cheng, X. D. Xiang, G. F. Dionne, S. F. Xu, J. He, Y. S. Chu, S. D. Preite, S. E. Lofland, and I. Takeuchi, Appl. Phys. Lett. **86**, 042506 (2005).

[31] J. He, S. F. Xu, Y. K. Yoo, Q. Z. Xue, H. C. Lee, S. F. Cheng, X. D. Xiang, G. F. Dionne, and I. Takeuchi, Appl. Phys. Lett. **86**, 052503 (2005).

[32] S. Kohiki, Y. Murakawa, K. Hori, H. Shimooka, T. Tajiri, H. Deguchi, M. Oku, M. Arai, M. Mitome, and Y. Bando, Jpn. J. Appl. Phys. **44**, L979 (2005).

[33] T. Ohno, T. Kawahara, H. Tanaka, T. Kawai, M. Oku, K. Okada, and S. Kohiki, Jpn. J. Appl. Phys. **45**, L957 (2005).

[34] N. H. Hong, J. Sakai, N. T. Huong, and V. Brizé, J. Magn. Magn. Mater. **302**, 228 (2006).

[35] N. H. Hong, J. Sakai, N. T. Huong, and V. Brizé, Appl. Phys. Lett. **87**, 102505 (2005).

[36] G. Peleckis, X. L. Wang, and S. X. Dou, Appl. Phys. Lett. **89**, 022501 (2006).

[37] T. Nakamura, J. Phys. D: Appl. Phys. **49**, 045005 (2016).

[38] K. Homma and F. Izumi, J. Appl. Crystallogr. **44**, 1272 (2011).

[39] S. Kitagawa and T. Nakamura, *2023 IEEE International Magnetic Conference (INTERMAG), Sendai, Japan* (IEEE, 2023), pp. 1–5.

[40] S. Kitagawa and T. Nakamura, J. Appl. Phys. **134**, 165302 (2023).

[41] S. Kitagawa and T. Nakamura (unpublished).

[42] A. Yasui, Y. Takagi, T. Osaka, Y. Senba, H. Yamazaki, T. Koyama, H. Yumoto, H. Ohashi, K. Motomura, K. Nakajima, M. Sugahara, N. Kawamura, K. Tamasaku, Y. Tamenori, and M. Yabashi, J. Synchrotron Rad. **30**, 1013 (2023).

[43] T. Nagata, O. Bierwagen, Z. Galazka, M. Imura, S. Ueda, H. Yoshikawa, Y. Yamashita, and T. Chikyow, Appl. Phys. Express **10**, 011102 (2017).

[44] T. Nagata, O. Bierwagen, Z. Galazka, M. Imura, S. Ueda, Y. Yamashita, and T. Chikyow, Jpn. J. Appl. Phys. **58**, SDDG06 (2019).

[45] T. Nagata, T. Yamaguchi, S. Ueda, W. Yi, J. Chen, T. Kobayashi, H. Yokoo, T. Honda, Y. Yamashita, and T. Chikyow, Jpn. J. Appl. Phys. **59**, SIIG12 (2020).

[46] M. Fondell, M. Gorgoi, M. Boman, and A. Lindblad, J. Electron Spectrosc. Relat. Phenom. **195**, 195 (2014).

[47] T. Nagata, O. Bierwagen, Z. Galazka, S. Ueda, M. Imura, Y. Yamashita, and T. Chikyow, Jpn. J. Appl. Phys. **58**, 080903 (2019).

[48] G. D. Mahan, Phys. Rev. B **25**, 5021 (1982).

[49] Y. Yonamoto, T. Yokoyama, K. Amemiya, D. Matsumura, and T. Ohta, Phys. Rev. B **63**, 214406 (2001).

[50] B. Gilbert, B. H. Frazer, A. Belz, P. G. Conrad, K. H. Nealson, D. Haskel, J. C. Lang, G. Srajer, and G. De Stasio, J. Phys. Chem. A **107**, 2839 (2003).

[51] J.-S. Kang, G. Kim, S. C. Wi, S. S. Lee, S. Choi, Sunglae Cho, S. W. Han, K. H. Kim, H. J. Song, H. J. Shin, A. Sekiyama, S. Kasai, S. Suga, and B. I. Min, Phys. Rev. Lett. **94**, 147202 (2005).

[52] R. Qiao, T. Chin, S. J. Harris, S. Yan, and W. Yang, Curr. Appl. Phys. **13**, 544 (2013).

[53] P. D. C. King, T. D. Veal, D. J. Payne, A. Bourlange, R. G. Egdell, and C. F. McConville, Phys. Rev. Lett. **101**, 116808 (2008).

[54] C. Körber, V. Krishnakumar, A. Klein, G. Panaccione, P. Torelli, A. Walsh, J. L. F. Da Silva, S.-H. Wei, R. G. Egdell, and D. J. Payne, Phys. Rev. B **81**, 165207 (2010).

[55] H. Raebiger, S. Lany, and A. Zunger, Phys. Rev. B **79**, 165202 (2009).